(NASA-TM-82497) TOLERANCE REQUIREMENTS TO PREVENT FLUID LEAKAGE IN THE CRUCIBLE/PLUNGER MEA EXPERIMENT MPS 770030 (NASA) 27 p HC A03/MF A01 CSCL 22A

N83-10094

Unclas
G3/12 38339

NASA TECHNICAL MEMORANDUM

NASA TM - 82497

TOLERANCE REQUIREMENTS TO PREVENT FLUID LEAKAGE IN THE CRUCIBLE/PLUNGER MEA EXPERIMENT MPS 770030

By Thomas J. Rathz
Space Science Laboratory

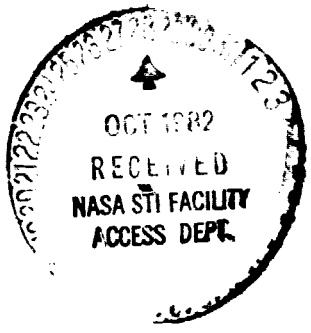

August 1982

NASA

George C. Marshall Space Flight Center
Marshall Space Flight Center, Alabama

TECHNICAL REPORT STANDARD TITLE PAGE

1. REPORT NO.	2. GOVERNMENT ACCESSION NO.	3. RECIPIENT'S CATALOG NO.
NASA TM-82497		

4. TITLE AND SUBTITLE	5. REPORT DATE
Tolerance Requirements to Prevent Fluid Leakage in the Crucible/Plunger MEA Experiment MPS 770030	August 1982
	6. PERFORMING ORGANIZATION CODE

7. AUTHOR(S)	8. PERFORMING ORGANIZATION REPORT #
Thomas J. Rathz	

9. PERFORMING ORGANIZATION NAME AND ADDRESS	10. WORK UNIT NO.
George C. Marshall Space Flight Center Marshall Space Flight Center, Alabama 35812	11. CONTRACT OR GRANT NO.
	13. TYPE OF REPORT & PERIOD COVERED
12. SPONSORING AGENCY NAME AND ADDRESS	Technical Memorandum
National Aeronautics and Space Administration Washington, D.C. 20546	14. SPONSORING AGENCY CODE

15. SUPPLEMENTARY NOTES

Prepared by Space Science Laboratory, Science and Engineering Directorate.

16. ABSTRACT

The work described was motivated by the unexpected leakage of molten Al-In out of the crucible of a proposed MEA materials processing in space experiment. The molten metals use a spring-loaded plunger to eliminate most free surfaces. The critical criteria necessary to initiate flow and the rate of fluid flow into the crucible/plunger annulus is calculated. Experimental in situ X-radiographs are interpreted according to the calculations. Also presented is a short note on possible effects of capillary flow if wetting occurs between crucible/plunger and liquids.

17. KEY WORDS	18. DISTRIBUTION STATEMENT
Isothermal solidification Materials Experiment Assembly (MEA) Fluid leakage Materials Processing in Space Experiments	Unclassified — Unlimited /Thomas J. Rathz

19. SECURITY CLASSIF. (of this report)	20. SECURITY CLASSIF. (of this page)	21. NO. OF PAGES	22. PRICE
Unclassified	Unclassified	26	NTIS

ACKNOWLEDGMENTS

The author wishes to express his gratitude for the discussions of the physical processes and mathematics of dynamic fluid flow with C. F. Schafer and for the enlightening talks with D. O. Frazier on various properties of immiscible metal systems relevant to this report. The author would also like to acknowledge the efforts of Mr. Edward Risch for the X-radiographs and Mr. Bill Aldrich for the use of his skills involving the furnaces.

TABLE OF CONTENTS

LIST OF TABLES

LIST OF ILLUSTRATIONS

SYMBOLS

$\mathbf{v}$	Velocity vector
ρ	Fluid density
t	Time
ν	Coefficient of kinematic viscosity
P	Pressure
X	Body force per unit mass
r, θ, z	Radial, azimuthal, and axial cylindrical coordinates
μ	Coefficient of viscosity
h	Height of fluid column from initial equilibrium
Δz	Distance of plunger travel from initial equilibrium
D_c	Diameter of crucible
D_p	Diameter of plunger
a	Annular gap between plunger and crucible
T	Temperature
g	Gravitational constant
σ	Liquid surface tension
ΔP	Interfacial disjoining pressure

TECHNICAL MEMORANDUM

TOLERANCE REQUIREMENTS TO PREVENT FLUID LEAKAGE IN THE CRUCIBLE/PLUNGER MEA EXPERIMENT MPS 770030

INTRODUCTION

The Materials Experiment Assembly (MEA) is an assembly of various materials processing furnaces capable of providing experimenters with the opportunity to perform materials science and fluid dynamics investigations for an extended period of time in the low-g environment of the Space Shuttle [1]. The first MEA flight is presently scheduled for the seventh Shuttle voyage. Among the set of experiments to be flown on MEA-1 will be the processing of the Al-In immiscible system. This experiment was originally flown on two separate Space Processing Application Rocket (SPAR) flights in an attempt to form a highly uniform dispersion of one phase within the other [2]. However, because of incomplete sample homogenization and possibly unexpected separation mechanics, a uniform dispersion in the solid state was not achieved. One of the particular processing modes that will be attempted on MEA with this same alloy system and is the concern of this report is the isothermal solidification of two sample compositions: Al-90 wt. pct. and 40 wt. pct. In.

The configuration to be used for the Al-90 w/o In and Al-40 w/o In cartridges is shown in Figure 1. Figure 1 is the Al-90 w/o In drawing while the Al-40 w/o In cartridge is different only in the interchanging of the alumina crucible/plunger with SiC-coated graphite components. The purpose of this change is to allow the majority phase liquid of each sample composition to preferentially wet the crucible/plunger and thus reduce the surface energy driven separation process. To further reduce surface tension driven separation, a spring-loaded plunger will contact the liquid metals and eliminate most of the free surface that would exist otherwise. Thus in a low-gravity environment the major separation processes such as Stoke's sedimentation, gravity-driven convection, and any free-surface Marangoni convection should be drastically reduced.

Because there existed a problem with reaching the requested 970°C soak temperature in the MEA furnace, some concern was expressed over attaining an initially homogeneous liquid at a new soak temperature of 860°C for the same soak time. Therefore, an Al-90 w/o In cartridge was processed at Marshall Space Flight Center having in situ X-radiography performed with the intent of learning the extent of sample homogenization taking place at the new soak temperature. However, as the sample materials became molten it was apparent from the X-rays that severe leakage of this liquid had occurred in the annular region between the plunger and the crucible. The plunger cavity region had almost become completely filled with the sample liquid. This leakage raised the questions of how much fluid flow would occur during different periods of time and temperatures as factors such as the plunger/crucible gap and spring force are varied. Such an analysis, as presented in this report, was deemed necessary for cartridge design and to prevent possible adverse effects on the scientific objectives.

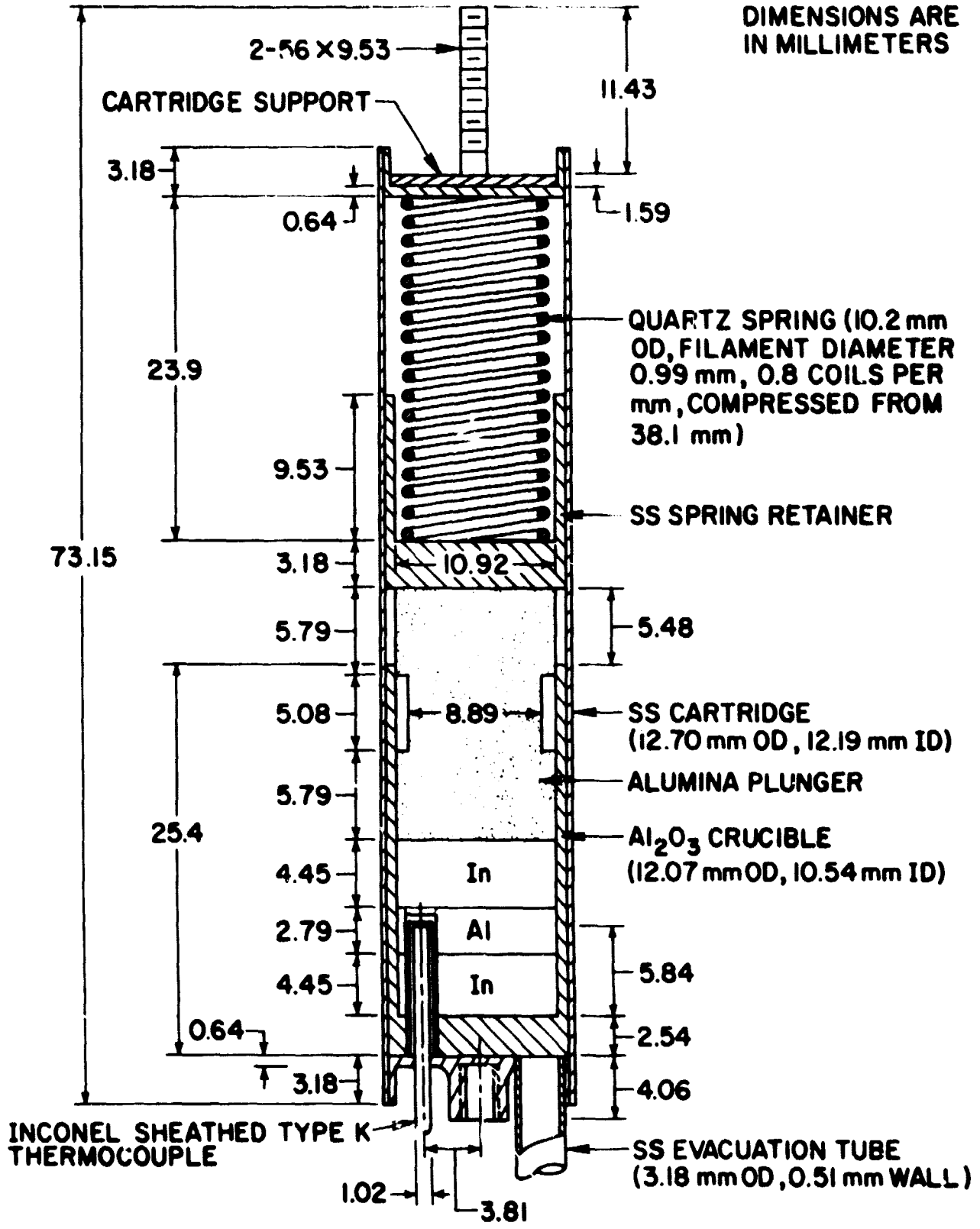

Figure 1. Cartridge configuration for Al-90 w/o In liquid immiscible experiment to be flown in MEA-1's isothermal furnace.

FLUID FLOW CALCULATIONS

The cartridge configuration shown in Figure 1 for this experiment had problems of molten sample leaking between the plunger and crucible. To present a more realistic view of the crucible/plunger/sample configuration, Figure 2 was drawn showing the dimensional variables that will occur in the calculations. Although Figure 2 is a simplification of Figure 1, none of the geometrical parameters that will enter into the calculations have been eliminated. The objective is to calculate mass flow rates for various gap sizes, a, which forms the annular region, for various total (spring) forces, F, and for various temperatures, T. The diameter of the crucible, D_c, will be held constant while the plunger diameter, D_p, is determined by the chosen gap size.

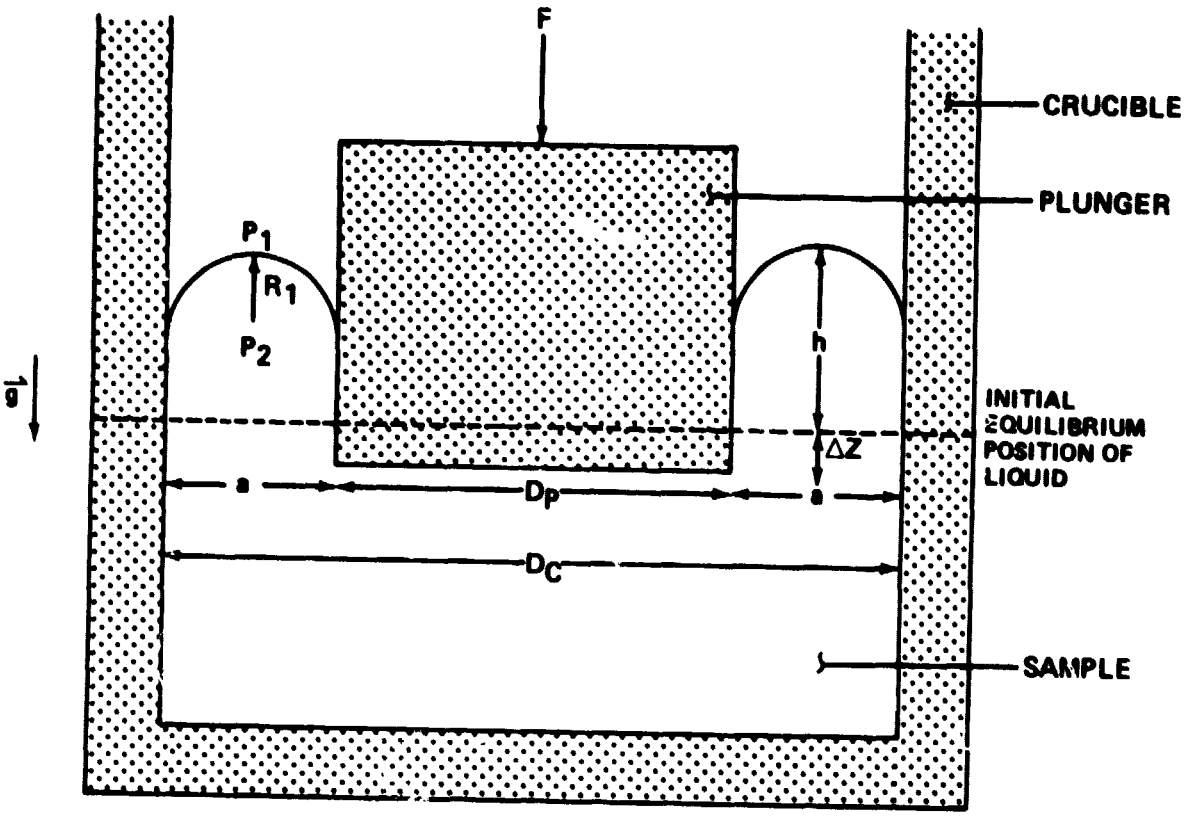

Figure 2. Cross sectional view of a simplified drawing of Figure 1 showing fluid flow into annular gap region.

The general Navier-Stokes equation for viscous incompressible flow which describes molten metals very well is given as

$$\frac{D\vec{v}}{Dt} = \frac{\partial \vec{v}}{\partial t} + \vec{v} \cdot \nabla \vec{v} = \vec{X} - \frac{\nabla P}{\rho} + \nu \nabla^2 \vec{v} \qquad (1)$$

where:

ρ = fluid density

$\vec{v}$ = velocity vector

t = time

ν = coefficient of kinematic viscosity

P = pressure

$\vec{X}$ = body force per unit mass.

Since this formidable equation cannot be solved analytically, it must be reduced to a form that can be dealt with. To do this requires an analysis of the magnitude of each term in equation (1) using appropriate assumptions, constraints, or boundary conditions.

The most obvious assumption to be made for the configuration shown in Figure 2 is to assume that steady state flow has been attained in the annular region. This results in

$$\frac{\partial v}{\partial t} = 0 \quad . \tag{2}$$

If cylindrical coordinates are chosen because of the problem's geometry, then another set of constraints that will be used are the following:

$$v_r = v_\theta = 0 \tag{3a}$$

$$P = P(z) \quad . \tag{3b}$$

Application of equations (3a) and (3b) to the following continuity equation

$$\frac{\partial v_r}{\partial r} + \frac{1}{r}\frac{\partial v_\theta}{\partial \theta} + \frac{\partial v_z}{\partial z} = -\frac{\rho v_r}{r} \tag{4}$$

results in the further restraint that

$$\frac{\partial v_z}{\partial z} = 0 \quad .$$

That is, the only flow that will occur is a constant flow in the z-direction and the velocity of this flow will depend only upon its radial position within the annulus (Fig. 3). Also, the pressure will depend only on the z-direction. Equation (3a) implies that

$$\frac{\partial v_r}{(\partial\theta, \partial r, \partial z)} = \frac{\partial v_\theta}{(\partial\theta, \partial r, \partial z)} = 0$$

and equation (3b) implies that

$$\frac{\partial v_z}{(\partial\theta, \partial z)} = 0 \quad .$$

Equation (1) now becomes in cylindrical coordinates:

$$\frac{Dv_r}{Dt} - \frac{v_\theta^2}{r} = X_r - \frac{1}{\rho}\frac{\partial P}{\partial r} + \nu\left(\nabla^2 v_r - \frac{v_r}{r^2} - \frac{2}{r^2}\cdot\frac{\partial v_\theta}{\partial\theta}\right)$$

$$\frac{Dv_\theta}{Dt} + \frac{v_r v_\theta}{r} = X_\theta - \frac{1}{\rho r}\frac{\partial P}{\partial\theta} + \nu\left(\nabla^2 v_\theta - \frac{2}{r^2}\cdot\frac{\partial v_r}{\partial\theta} - \frac{v_\theta}{r}\right) \qquad (5)$$

$$\frac{Dv_z}{Dt} = X_z - \frac{1}{\rho}\frac{\partial P}{\partial z} + \nu\nabla^2 v_z$$

where by definition:

$$\frac{D}{Dt} = v_r\frac{\partial}{\partial r} + \frac{v_\theta}{r}\frac{\partial}{\partial\theta} + v_z\frac{\partial}{\partial z} + \frac{\partial}{\partial t} \qquad (6)$$

$$\nabla^2 = \frac{1}{r}\frac{\partial}{\partial r}\left(r\frac{\partial}{\partial r}\right) + \frac{1}{r^2}\frac{\partial^2}{\partial\theta^2} + \frac{\partial^2}{\partial z^2} \quad .$$

Applying equations (2), (3a), and (3b) to equations (4) and (5) results in

$$v_z\frac{\partial v_z}{\partial z} = X_z - \frac{1}{\rho}\frac{\partial P}{\partial z} + \nu\nabla^2 v_z \qquad (7)$$

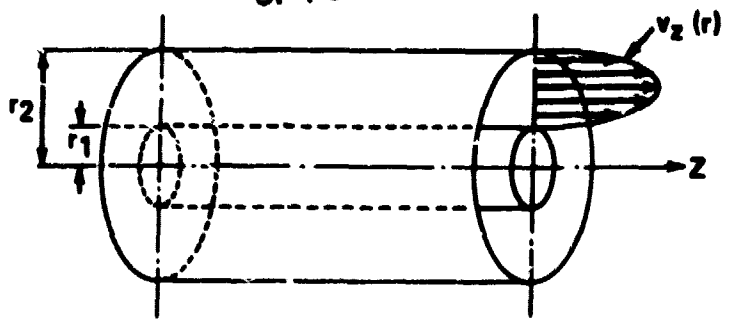

Figure 3. Velocity profile of a viscous fluid which flows steadily parallel to the axis in the annular region between two coaxial cylinders of radii r_1 and r_2.

for the Navier-Stokes equation. Using the continuity constraint from equation (4) finally gives

$$0 = X_z - \frac{1}{\rho}\frac{dP}{dz} + \nu \frac{\partial^2 v_z}{\partial z^2} \quad . \tag{8}$$

Since the only body force of concern to this problem is gravity and due to its orientation in Figure 2 we can thus reduce the dimensionality of equation (8) to two independent terms:

$$0 = A + \mu \left(\frac{\partial^2 v_z}{\partial r^2} + \frac{1}{r}\frac{\partial v_z}{\partial r} \right) \tag{9a}$$

where

$$A = \rho X_z(z) - \frac{dP(z)}{dz} \tag{9b}$$

is independent of r and μ is the coefficient of viscosity. If we now solve (9a) by applying the following boundary conditions

$$v_z = 0 \quad \text{at} \quad r = r_1, \quad \text{and} \quad r = r_2 \tag{10}$$

we obtain the velocity of fluid flow within an annulus between two coaxial cylinders

$$v_z(r) = \left(\frac{1}{4\mu} A\right)\left[\left(r_1^2 - r^2\right) + \frac{(n^2-1)r_1^2}{\ln(n)} \ln\left(\frac{r}{r_1}\right)\right] \qquad (11)$$

where $n = r_2/r_1$.

The quantity of most usefulness to examine is the mass flow rate which can be found from

$$\dot{m} = \rho \int_{\theta=0}^{2\pi} \int_{r=r_1}^{r=nr_1} v_z r \, dr \, d\theta \qquad (12)$$

$$= \frac{\pi r_1^4 \rho A}{8\mu}\left[(n^4 - 1) - \frac{(n^2 - 1)^2}{\ln(n)}\right] . \qquad (13)$$

Note that $\dot{m}$ is proportional to F through dP/dz in A, where F is the force on the piston. A big assumption in the derivation of $\dot{m}$ is the neglect of the effects the moving plunger will have on the boundary conditions of equation (10). This effect can be included in the boundary conditions but, as is shown below, this is small enough to be neglected. By conservation of volume flux, the relationship between the fluid height h and the downward distance Δz moved by the piston as shown in Figure 2 is given by

$$h/\Delta z = \frac{(D_c - 2a)^2}{4a(D_c - a)} \qquad (14)$$

which results in a range of values $20 \leq h/\Delta z \leq 518$ for $0.005 \text{ in.} \leq a \leq 0.0002 \text{ in.}$ Thus for the entire range of annular gap values, the plunger motion can indeed be neglected.

Since the magnitude of $\dot{m}$ in equation (13) depends upon A, the relative sizes of each term in A need be examined. The only body force to consider is that of the constant gravitational acceleration such that $X(z) = g$. Now the pressure gradient dP/dz is that pressure acting through a chosen distance, or height, of 1 cm due to the resultant forces of the spring and the masses of the retainer and plunger acting over the plunger-face area. These forces are summarized in Table 1 and when the spring force is compared to the maximum body force, the latter can be considered negligible for dynamic flows. However, this body force due to the plunger/retainer masses in 1-g amounts to approximately 10 percent of the spring force. This 10 percent additional force does not appear to be much until the static forces in Figure 4 are examined in the next paragraph.

TABLE 1. COMPONENT FORCES ACTING ON PLUNGER

	ρ (g/cc)	Volume (cc)	Force (dynes)	
			1-g	0-g
Alumina Plunger	3.96	1.298	5037	–
Graphite Plunger	1.85	1.298	2353	–
Spring Retainer (304 S. S.)	8.044	0.59	4655	–
Quartz Spring	–	–	1.1×10^5	1.1×10^5

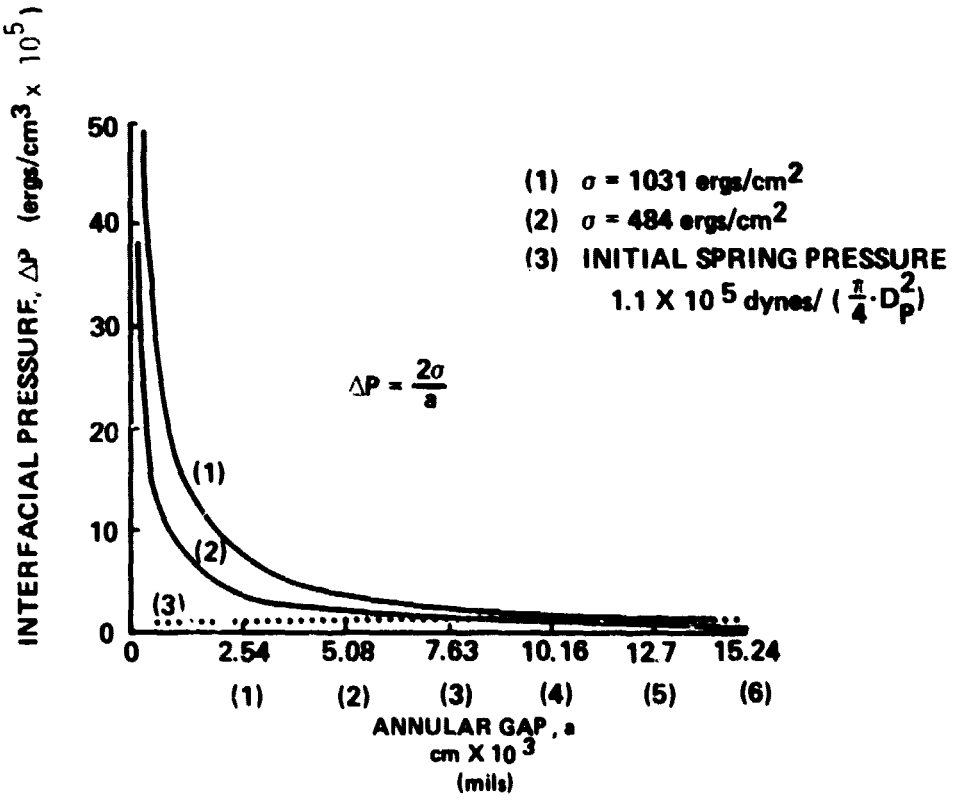

Figure 4. Interfacial pressure at the region of coexistence between the liquid alloy and external vapor as a function of the annular gap parameter for various liquid vapor surface tensions.

To initiate fluid flow, a static pressure larger than the interfacial pressures of Figure 4 is needed to form the meniscus since we have assumed no wetting of the container by the uids. Curves 1 and 2 are for values of the liquid surface tension spanning the set of values for the pure components [and thereby the (Al-In)-mixtures] for the range of temperatures used during the MEA experiments. Curve 3 shows the applied spring pressure: if curve 3 lies above curves 1 or 2, then flow could ensue. As can be seen, the 10 percent additional static force of the retainer/plunger masses in 1-g will be a critical factor. Also, since flow has been observed in ground based experiments performed with cartridges as designed in Figure 1, then either the spring force or the annular gap was larger than expected, or the additional mass forces caused the problem. Since the latter is a 1-g effect, this paper concentrated on the effects of the possible variations in the spring force on the flow rate, $\dot{m}$, in zero-gravity as a function of annular gap.

The following calculations of $\dot{m}$ used the thermophysical data of Table 2 and the following assumptions:

- The pressure gradient producing flow was only due to the spring force (nominally 10^5 dynes) acting over a 1-cm distance; and most importantly, this force was big enough to overcome the liquid disjoining pressure detailed in Figure 4.

- The crucible inside diameter was 1.054 cm.

- The plunger was concentric with the crucible and thus eliminated any possible frictional forces between crucible/plunger.

- No wetting of the crucible/plunger by the liquid phases took place which would have allowed capillary flow (see appendix).

- The annular gap opens into a larger area into which the fluid flowed so that the interfacial pressure was not a factor in the dynamic flow up the 1-cm height.

- Hydrostatic body forces were negligible.

- Distance traveled and motional effects of plunger were negligible compared to height or speed of liquid flow rate.

The results of the calculations are shown in Figures 5 through 7. Figure 5 shows the relative size of the mass flow rate for the various liquid metals at a temperature of 1000°C and spring force of 10^5 dyne. Even though the density and viscosity of equation (13) each have their own separate temperature dependence, it is the kinematic viscosity (μ/ρ) which causes several of the curves in Figure 5 to nearly overlay one another. As expected, however, the higher viscosity of Al causes a slower rate of loss. The curves fall well within a factor of 5 of each other at any particular gap value.

Figures 6a through 6d show the temperature dependence of the mass flow rate of the (Al, In) liquids of interest for a spring force of 10^5 dynes. As expected, the flow rate increases with temperature for a particular material due to the decreasing exponential temperature dependence of the viscosity as opposed to the decreasing linear dependence of the density in the models used. Approximately 40 percent difference exists in flow rates for a temperature difference of 300°C for a particular material. Because In has a lower melting temperature than the other Al or Al-In

TABLE 2. CALCULATED THERMOPHYSICAL PROPERTIES FOR (In, Al) LIQUIDS

	Al-40 w/o In			Al-90 w/o In			Pure In			Pure Al		
Temperature (C)	σ	ρ	μ	σ	ρ	μ	σ	ρ[a]	μ[a]	σ	ρ[a]	μ[a]
200	-	-	-	-	-	-	556	6.99	0.0164	-	-	-
600	-	-	-	-	-	-	520	6.72	0.0075	-	-	-
700	763	3.19	0.0141	592	5.64	0.01	511	6.65	0.0069	816	2.37	0.0115
1000	638	3.05	0.0068	537	5.46	0.006	484	6.45	0.0057	666	2.29	0.0071
Ref.	4[b]	4	4	4[b]	4	4	3	5	5	3	5	5

Units: σ = surface tension (ergs/cm^2); ρ = density (g/cc); μ = viscosity (dyne-s/cm^2)

a. $\rho_{Al} = 2.385\ (T-660.1)\ (2.8 \times 10^{-4})$; $\rho_{In} = 7.023-(T-156.6)\ (6.8 \times 10^{-4})$
$\mu_{Al} = 0.001492 \exp\ [16.5 \times 10^3/8.3144(T')]$; $\mu_{In} = 0.00302 \exp\ [6.65 \times 10^3/8.3144(T')]$
T' = temperature (K), T = temperature (C)

b. Calculations based on Guggenheim model.

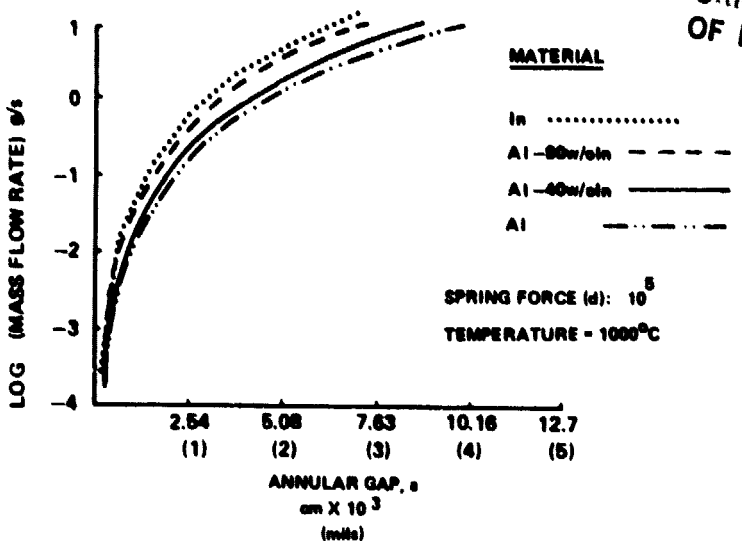

Figure 5. Calculated mass loss rate versus annular gap for several Al-In compositions at 1000°C and 10^5 dynes of spring force.

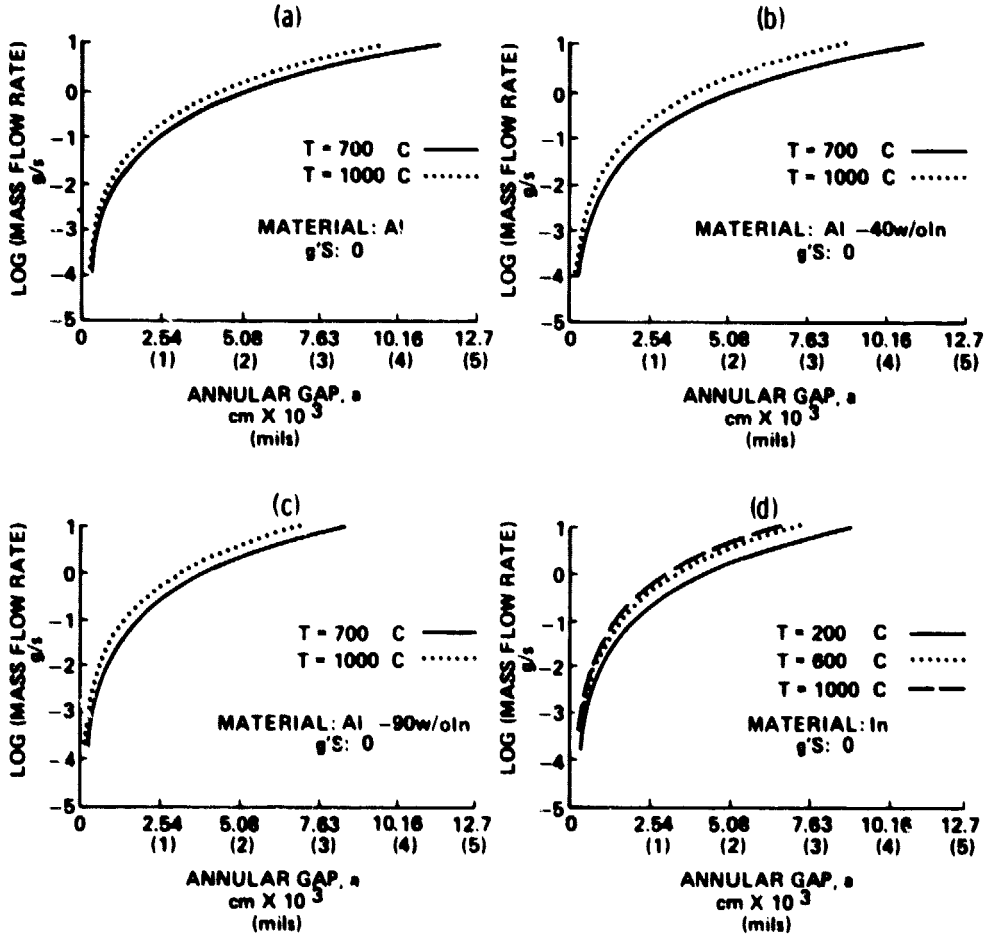

Figure 6. Calculated mass loss rate versus annular gap at various temperature and at 10^5 dynes of spring force for (a) pure Al, (b) Al-40 w/o In, (c) Al-90 w/o In, and (d) pure In.

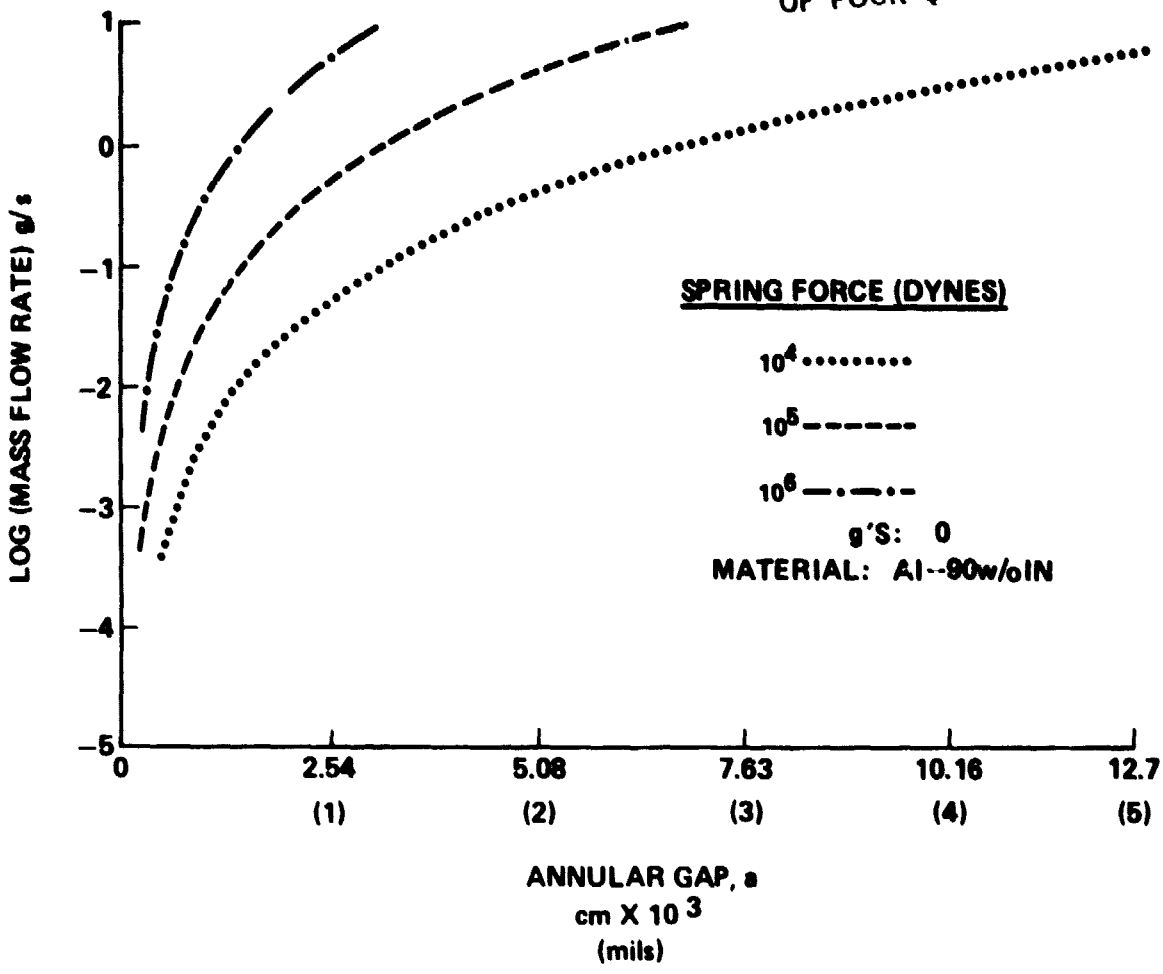

Figure 7. Calculated mass flow rate versus annular gap for Al-90 w/o In at 1000°C and at various spring forces.

alloys, three curves are illustrated in Figure 6d. The pure Al and In figures are presented because of the possibility of having In fluid flow into the annular gap (Fig. 1) before the Al melts and mixes; or, the possibility exists of having the molten Al segregate to the top of the sample and thereby having the Al flow into the gap.

To illustrate the effects of various spring forces, Figure 7 presents the Al-90 w/o In material at 1000°C for spring forces of 10^4, 10^5, and 10^6 dynes. Again, as expected from equation (13), an order of magnitude variation in the spring force causes an equal order of magnitude change in the flow rate.

Some general comments about the entire set of graphs should be made concerning the magnitude of the mass flow rate. At the most conservative values of flow rate (approximately 0.1 g/sec for Al at 700°C and $F_s = 10^4$ dynes) and for a typical Al 90 w/o In cartridge annular gap value of 5.08×10^{-3} cm (2 mils), the entire volume of metal would be squeezed out of the crucible in less than 100 sec. A second comment concerns the sensitivity of the mass flow rate (MFR) to the gap size. A 2.54×10^{-3} cm (1 mil) change in the gap can increase the MFR by almost an order of

magnitude; however, at smaller gap values this is no longer true. At these smaller values, the slope is such that any small uncertainties in the gap value (which will most likely occur in crucible/plunger machining processes) will produce large uncertainties in the MFR, although the overall magnitude of the MFRs will still be quite low. This latter effect is particularly expected for the Al-40 w/o In cartridges whose annular gap is supposed to be about 1.27×10^{-3} cm (0.5 mils).

OBSERVED FLOWS

As stated in the introduction, MEA ground based experiments were performed in which in situ X-radiographs were taken at critical temperatures during the processing of both Al-40 w/o and 90 w/o In samples. From these radiographs can be seen several of the effects discussed in the previous section. Figure 8a shows the processing of cartridge P-4 (Al-90 w/o In: alumina crucible/plunger) at the monotectic temperature of 640°C during heat-up; although nonuniform, flow has begun. The "bubbles" are of In and are forming in the plunger cavity region. Thus the critical vapor-liquid surface tension discussed in Figure 4 has been exceeded so that flow can commence. As seen in Figure 8a, the density inversion of the Al and In layers will cause some Al to be forced into the gap and up into the plunger cavity. As evidenced in Figure 8b at T = 820°C, the Al-rich and In-rich phases in the plunger cavity are now beginning to separate upon cooling from a soak time/temperature of 8 hr/860°C.

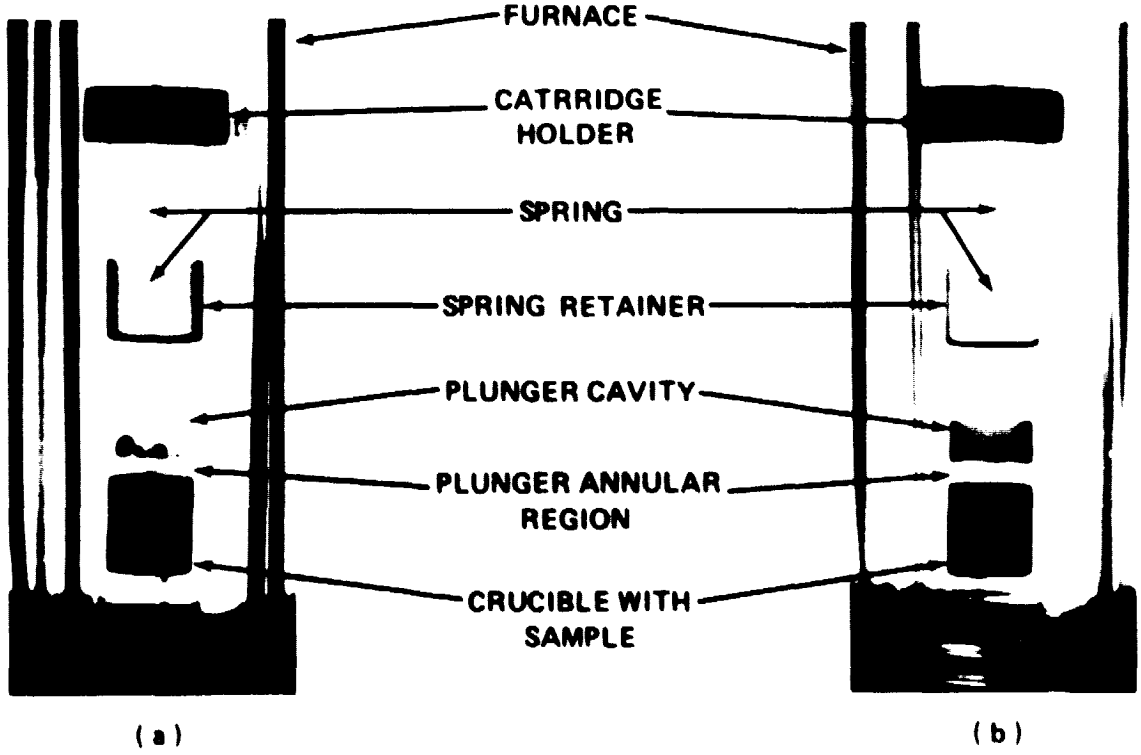

Figure 8. Radiograph of cartridge P-4, Al-90 w/o In, with in furnace while (a) heating up to 640°C: localize flow through annular gap and into plunger cavity; sample density stratification beginning; (b) cooling down to 820°C where Al-In separation seen in plunger cavity.

There were several interesting phenomena observed in these radiographs. One surprise was the non-uniformity of the flow up the sides which suggest that there existed possible machining flaws in the plunger that provided non-uniform flow channels. The biggest surprise was the lack of steady flow of the entire volume of fluid out of the crucible. Since the spring constant and spring force were given as 8.8×10^4 dyne/cm and 1.1×10^5 dynes respectively, the expected travel distance allowable for the plunger would thus be 1.25 cm which is about the full depth of the crucible. Since this entire fluid drain was not observed, speculations such as plunger/crucible skewness, or vapor deposition and locking at the upper crucible/plunger junction, or other mechanisms can only be postulated to have stopped the plunger from advancing further.

In another Al-90 w/o In experiment, the sample (P-3) was run for 9.5 hr at 970°C. The greater amount of plunger bearing surface near the sample provided a slight variation in this experiment. However, as shown in Figure 9, the radiograph taken after processing indicates that partial flow again occurred but only along one side and not into the cavity. This provides indications that plunger/crucible skewness existed which could only provide flow along one side until the plunger is immobilized and flow is stopped. Skewness can stop flow by presenting a channel on one side of the plunger which is too narrow for surface tension to be overcome (Fig. 4). This critical width will be encountered at varying heights when the plunger is skewed with respect to the crucible. Even a reprocessing of this same cartridge at 970°C for 1 hr in a figure 1-inverted position failed to cause any changes in the fluid profile of Figure 9. This inverted processing lends credence to the negligible effect of gravity compared to the spring force on the fluid flow in the annular gap.

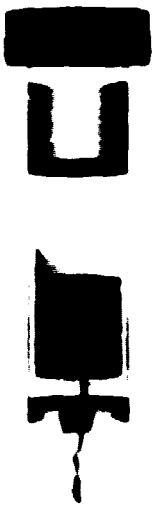

Figure 9. Radiograph of cartridge P-3, Al-90 w/o In at room temperature after processing at 970°C for 9.5 hr. Non-uniform flow along one side of plunger.

Finally there were two Al-40 w/o In cartridges which were processed. In situ X-radiographs taken of one cartridge (S-2) processed at 880°C for 3.5 hr and X-radiographs taken of another (S-3) after processing at 960°C for 9 hr showed no evidence of fluid flow (Fig. 10). This could be expected from the smaller annular

Figure 10. Radiograph of cartridge S-3, Al-40 w/o In at room temperature after processing at 960°C for 9 hr. No observable flow.

gap of less than 2.54×10^{-3} cm (1 mil) and the implications thereby provided from Figure 4. Even though the Al was invisible because of the X-ray intensity used, any flow of the Al-In mixture would have been readily seen. One side comment must be made concerning the somewhat dispersed appearance of the Al-In solid seen in Figure 10. Some separation is seen in Figure 10 but not as complete as that seen in the room temperature radiographs of samples P-4 and P-3 (Fig. 9) or in any previous Al-In ground base (1-g) experiments which have always been performed with very large free surfaces available, i.e., non-plunger configuration [2]. This effect will be further investigated and reported later.

SUMMARY

From the calculations performed for the cartridge configuration of Figure 1, the onset of fluid flow can be determined from various experimental parameters. The overall critical criteria is the data presented in Figure 4 in which the spring force must initially overcome the disjoining pressure of the liquid-vapor interface at the gap before flow can transpire. The maximum gap allowable beyond which flow occurs is presented in the following tabulation as a function of the applied spring force. Thus, it is crucial that the spring force be well known at all temperatures and the critical annular gap size be appropriately chosen. A prudent choice would be as small a gap as manufacturably possible so that if the critical gap is met, then flow will be as minimal as possible. However, the potential exists for attaining a critical frictional force between the greater crucible and plunger contact surface area as the gap size is reduced which may entirely inhibit plunger motion. This can be determined by laboratory test.

The variances in the sample's thermophysical properties and the spring force do not produce as great a change in the computed mass flow rates as compared to the variances in the annular gap value. This result is exemplified in the observed flows.

Force ($d \times 10^{-5}$)	Critical Maximum Annular Gap ($cm \times 10^{3}$)	(mils)
0.5	15.9	6.3
1.0	8.2	3.2
1.5	5.5	2.2
2.0	4.2	1.6
2.5	3.3	1.3
3.0	2.8	1.1

As seen in the Al-90 w/o In cartridges, fluid flow is fairly prevalent but not continuous nor uniform. This suggests a halting of the plunger motion by a possible skewness with the crucible. The Al-40 w/o In showed no signs of flow which suggest that the smaller gap value for these cartridges presents a surface tension barrier to flow, as suggested by Figure 4.

Since the publication of this paper, the experimental cartridges will have already been redesigned to insure that a maximum gap value of 1.2×10^{-3} cm (0.5 mil) is used for both Al-In compositions. It is hoped that no leakage into the gap occurs because any leakage will cause an unknown amount of shift in the initial composition of the alloy and thus have detrimental effects on the relative volume percentages of each immiscible phase. With relative composition unknown, modeling any observed separation that occurs will be rendered difficult or impossible. The inhibition of fluid flow beyond the plunger cavity by reducing the annular gap will also provide some margin of safety for the flight furnace by not having Al-In react through the stainless steel cartridge; but, any flow will still be deleterious to scientific analysis.

APPENDIX

In a report by Potard [6], SiC is wetted by aluminum ($\theta_{Al} < 90$) preferentially over that of indium; also, the monotectic composition wets the SiC. However, Löhberg, et al. [7] claim that neither the Al nor In wets alumina ($\theta_{Al}, \theta_{In} > 90$). Since one phase (Al) is reported to wet the crucible, and since there exist the possibility of attaining a critical temperature at which any of the other phases may wet the crucibles [8], it was decided to analyze the capillary flow that would occur in the annular gap assuming the entire Al-In composition range wets the crucibles. The following analysis is based on the simple discussion of Bourgeouis [9].

The flow equation in the annular gap region for capillary flow and no forced flow is

$$v = \frac{\rho g\, r_2^2\, \phi}{8 \mu h} (h_o - h) \qquad \text{(A-1)}$$

where

$$\phi = \frac{1 - n^4}{1 - n^2} + \frac{1 - n^2}{\ln(n)} \qquad \text{(A-2)}$$

$$h_o = \frac{2\sigma \cos \theta}{\rho g\, r_2 (1 - n)} \qquad \text{(A-3)}$$

and v, μ, ρ, g, n, r_2, and σ are as previously defined; also, h = axial position in annulus. The quantity h_o is the equilibrium height of capillary rise counter-balanced by the pressure gradient established by gravity, g. Therefore, the position h, which is to be the reference point from which v is computed, must be less than h_o; this forms a constraint in the computations. For this report's purpose the previously used 1 cm maximum height was chosen for h. The mass flow rate for this problem was simply taken as

$$\dot{m} = \rho v A \qquad \text{(A-4)}$$

where A is cross sectional area of annular region.

Using the same thermophysical data of Table 2 as used for the previous non-wetting flow rate calculations, the following analysis is presented. The variables to alter are the g-level, the wetting angle, the material's thermophysical data, and the annular gap value.

Figure 11 presents the mass flow rate (MFR) for the various materials at 1000°C, wetting angle of 75 deg, and at 1-g of gravity for various annular gap values. The various material properties give MFRs within 50 percent of each other at any particular gap value. Note that the MFRs are about the same order of magnitude and functionally equivalent to the MFRs of Figure 5; this is as expected since the only major difference between the flows described by equation (A-4) versus (13) is the type of force causing the flow. Also noticeable is the MFR's dependency on the wetting angle as shown in Figure 12. Note the dramatic reduction in MFR as the limit of wetability is approached, i.e., as $\theta \rightarrow 90$ deg.

Finally, the effect of temperature and gravity can both be seen in Figure 13. For a particular set of conditions, the MFR will vary by about 50 percent for a temperature change of 300 deg. The MFR for a 10^{-4} g-level diverges as the annular gap increases so that there is no constant value for the amount of change that occurs. For this problem, the g level makes very little contribution to the MFR until $g \gg 1$-g.

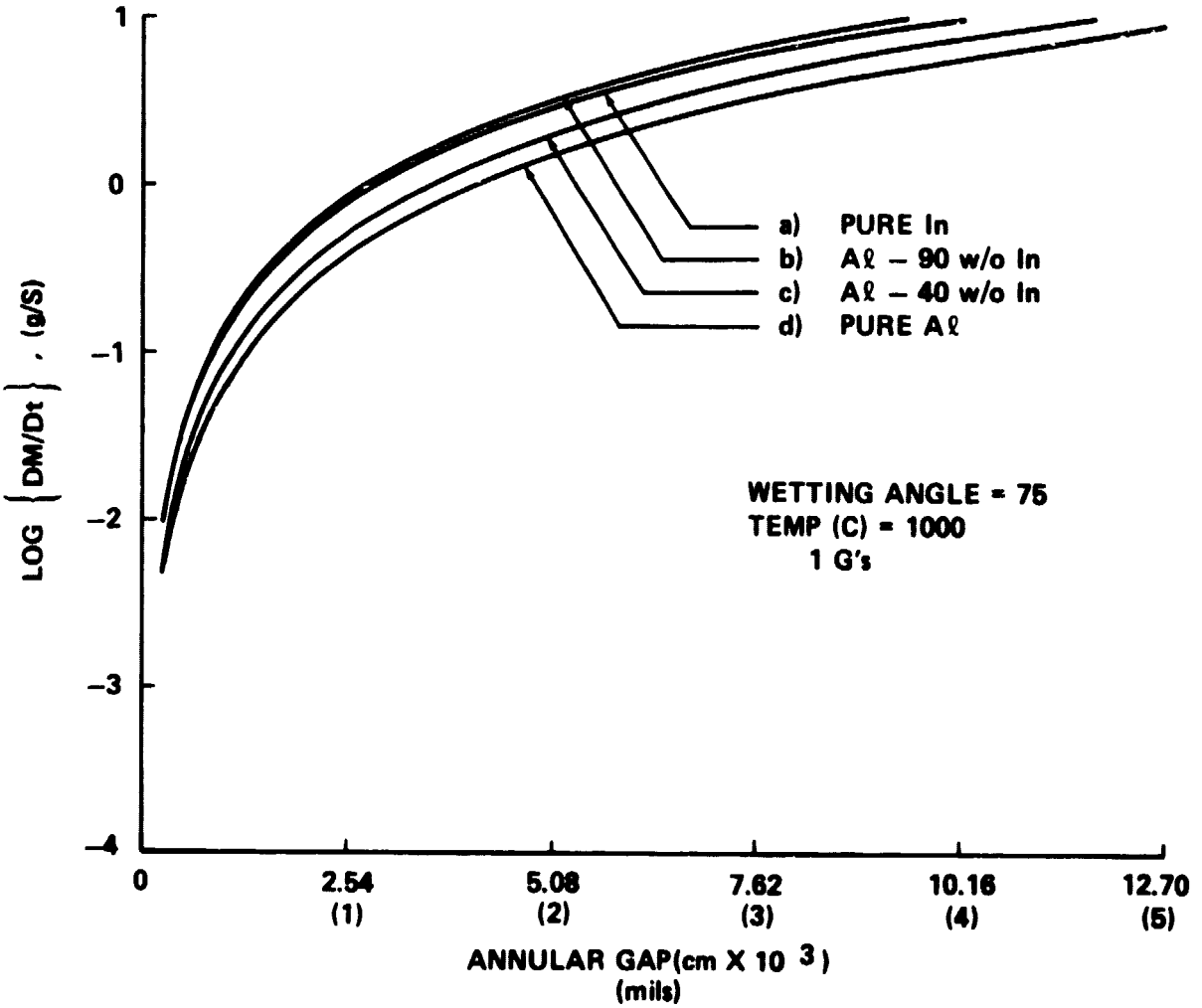

Figure 11. Capillary flow versus annular gap at $\theta = 75$ deg and temperature of 1000°C for (a) pure In, (b) Al-90 w/o In, (c) Al-40 w/o In, and (d) pure Al.

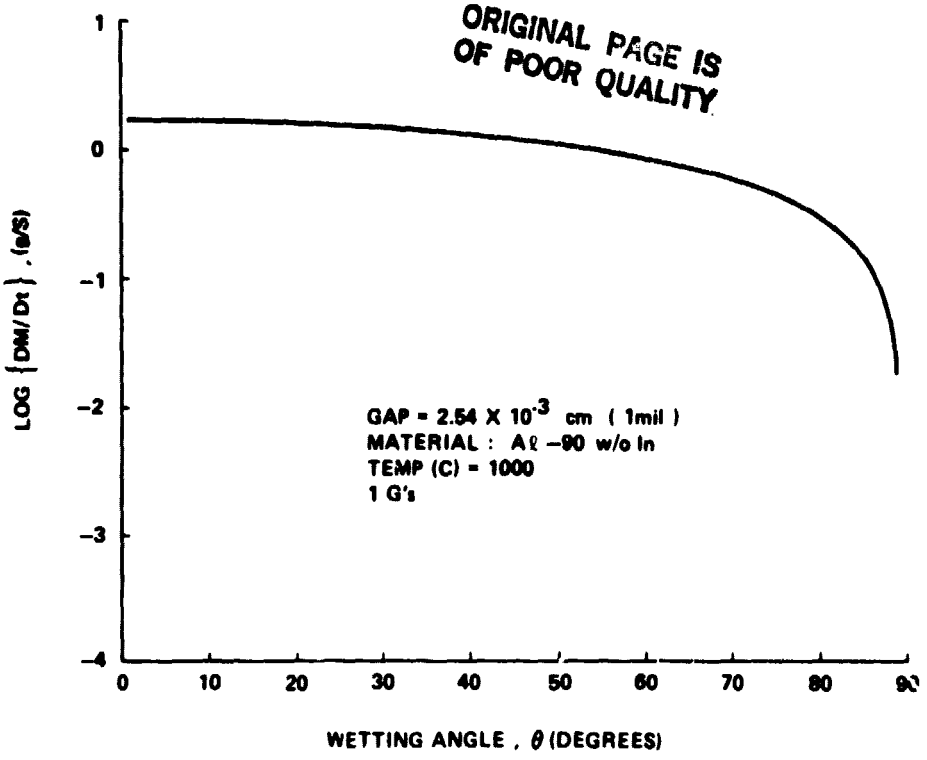

Figure 12. Capillary flow rates versus wetting angle for a particular gap size, temperature, g-level, and material.

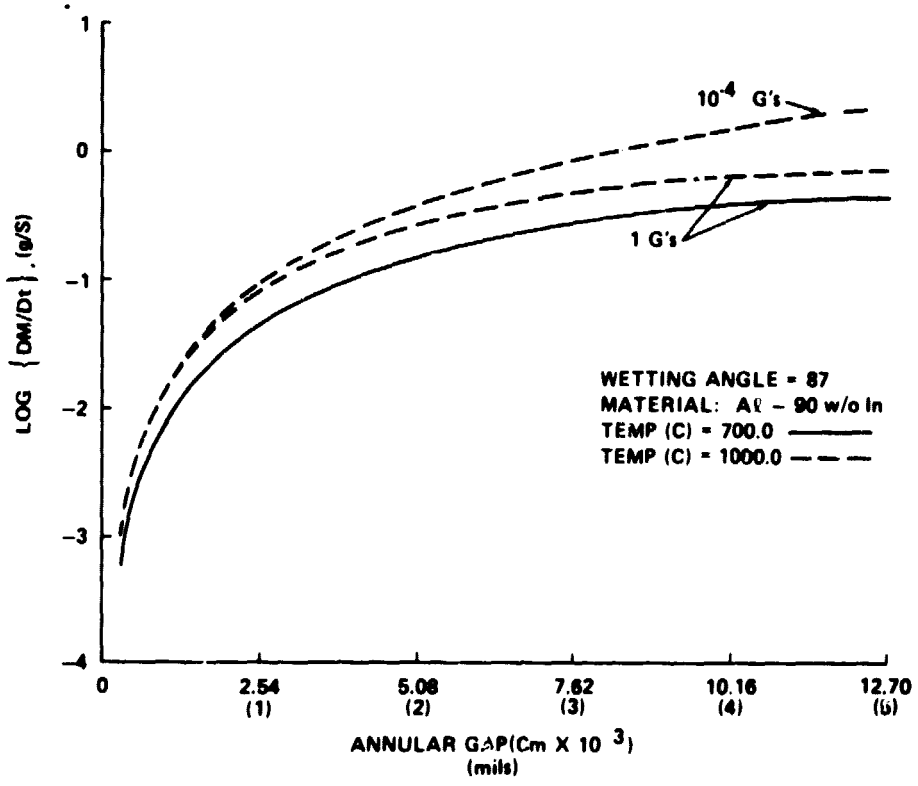

Figure 13. Capillary flow rates versus annular gap for two temperatures and two g-levels.

REFERENCES

1. Materials Experiment Assembly, Design and Performance Specification, MSFC-SPEC-951B, December 6, 1979.

2. Space Processing Applications Rocket Project – SPAR II Final Report, NASA TM-78125, Space Processing Applications Rocket Project – SPAR V Final Report, NASA TM-78275, 1980.

3. Murr, L. E.: Interfacial Phenomena in Metals and Alloys. Addison-Wesley Publishing Co., Reading, Massachusetts, 1975.

4. Gelles, S. H.: Calculated Thermophysical Properties of Select Al-In Alloys. December 1980 Report, NASA Contract NAS8-32952. 22nd Monthly Progress Report, March 1980.

5. Smithells, C. J. and Brandes, E. A.: Metals Reference Book. 5th Edition, Butterworths, 1976.

6. Potard, C.: J. Brit. Inter. Soc., vol. 31, 1978, p. 275.

7. Löhberg, K., Dietl, V., and Ohlborn, H.: SPAR II Final Report. NASA Technical Memorandum TM78125, November 1977.

8. Cahn, J. W.: Met. Trans., vol. 10A, 1979, p. 119.

9. Bourgeouis, S. V., Jr.: Phase B Report, NASA Contract NAS8-27015, July 1973.

APPROVAL

TOLERANCE REQUIREMENTS TO PREVENT FLUID LEAKAGE IN THE CRUCIBLE/PLUNGER MEA EXPERIMENT MPS 770030

By Thomas J. Rathz

The information in this report has been reviewed for technical content. Review of any information concerning Department of Defense or nuclear energy activities or programs has been made by the MSFC Security Classification Officer. This report, in its entirety, has been determined to be unclassified.

for W. C. McCarman

A. J. DESSLER
Director, Space Science Laboratory

☆U.S. GOVERNMENT PRINTING OFFICE 1982-546-071/72